ORIGINAL PAPER

Petrophysical characterization of the heterogeneous shale-rich oil reservoirs: a case study of the Cenomanian Clastics, Abu Sennan Concession, North Western Desert of Egypt

Ahmed H. Saleh[1] · Ahmed Henaish[1] · Fatma S. Ramadan[1] · Mohamed O. Abd El Fatah[2] · Mahmoud Leila[3]

Abstract

Shale-rich reservoirs present a long-standing challenge for reservoir geologists because the clay minerals often induce a large-scale heterogeneity in the reservoir pore system. This work aims to understand the impact of clay distribution and mineralogy which would enhance the predictability of the best reservoir facies. We integrate seismic, well-log datasets to investigate the petrophysical characteristics of the clay-rich Cenomanian Clastics in the GPY oil field, north Western Desert of Egypt. These Clastics comprise the sandstone intervals which are the most prolific hydrocarbon reservoirs. Seismic data were used to interpret the main structural patterns as well as the different seismic facies. The well log data were utilized to interpret the lithologic variations and the type of clays in the reservoir as well as the different petrophysical parameters. Based on variations in their lithological and petrophysical characteristics, the Bahariya sandstones were sub-divided into three different rock units: Bahariya-3 (B-3), Bahariya-2 (B-2), and Bahariya-1 (B-1), separated by thick laminated clay intervals. AR/G Member is dominated by clays with relatively lower reservoir quality. Spectral gamma ray log values reveal that smectite is the dominant clay mineral in all the studied intervals. Laminated clays are dominant in B-1 and B-2 units, whereas, B-3 unit and Abu Roash G Member are enriched in structural clays. The quartzose sand content decreases from B-3 to AR/G and clay content increases from B-3 to AR/G. Therefore, the best reservoir facies and fluid flow conduits with best pore system characteristics are hosted in B-3 and the smectite clay streaks act as a good seal for hydrocarbons in the quartzose sandstone pay zone.

Keywords Cenomanian · Abu Roash G · Bahariya · Petrophysical parameters · Clay type

Introduction

Clay minerals' distribution in reservoir rocks presents key challenges to exploration geologists because of their detrimental effect on the reservoir quality (e.g., Loucks et al. 1984; Ehrenberg 1990; Walderhaug et al. 2012; El Adl et al. 2021). However, recent studies highlighted the

---

✉ Ahmed H. Saleh
ahmohammed@zu.edu.eg

1 Geology Department, Faculty of Science, Zagazig University, Zagazig, Egypt

2 Exploration Department, Egyptian General Petroleum Company, Cairo, Egypt

3 Geology Department, Faculty of Science, Mansoura University, Mansoura, Egypt

beneficial impact of specific clay mineral phases on the reservoir quality such as chlorite coating in deeply buried reservoirs through preventing further diagenetic attributes such as quartz from destructing the primary porosity (e.g., Pittman 1992; Leila et al. 2018; Leila 2019). Therefore, the occurrence of clays and shale beds in the reservoir would complicate the determination and evaluation of petrophysical parameters. Accordingly, analyzing the type, content, and distribution mode of clay minerals in the reservoir is elemental for reservoir evaluation and management (Ghassem 2018; Spooner 2018). In Clastics reservoirs, clays occur in three distribution types comprising dispersed, laminated, and structural. Each type varies in its impact on the reservoir quality (Wei et al. 2014; Ghassem and Roozmeh 2017).

The Cenomanian Clastics including the Bahariya and Abu Roash G sediments present the most prolific reservoirs in the north Western Desert (EGPC 1992; Dolson et al. 2001; Kassab et al. 2019; Yasser et al. 2021). These sediments

were deposited in a paralic depositional environment, and therefore host thick successions of Clastics dominated by argillaceous sandstones (Yasser et al. 2021; Radwan et al. 2022). The present study is focused on the GPY oil field to the east of the Qattara Depression on the southern flank of the Abu Gharadig basin, Western Desert, Egypt (Fig. 1). Abu Gharadig basin is one of the most prolific basins in the whole Egypt as it contains the most productive oil and gas fields in the north of the Western Desert (El-Shaarawy et al. 1994; Teama and Nabawy 2016; Radwan et al. 2022). GPY field produces oil from the Cenomanian Bahariya and Abu Roash G (AR/G) sandstones. The drilling activity in this field started in 1981 by drilling an exploratory well named GPY-1 based on seismic data analysis and interpretation. This well produces 200 barrels of oil per day from the AR/G reservoir with an oil viscosity between 40 and 42 API (EGPC 1992). Except for GPY-11 and GPY-9, which are categorized as less productive wells, all other wells host significant hydrocarbon-bearing horizons in their sedimentary succession. However, these horizons are highly heterogeneous and most of the pay zones are laterally and vertically not connected due to the presence of numerous clay barriers. Moreover, Abu Roash G sandstones produce oil from some pay zones in specific wells and are dry in other wells typifying a large-scale reservoir heterogeneity. Therefore, the main objective of this study is to define the different petrophysical properties of the studied Cenomanian reservoirs and investigate their vertical and lateral distribution in the study region. Moreover, the impact of lithological attributes on the reservoir properties will be investigated. Additionally, the factors controlling the reservoir heterogeneity as well as the different scales of heterogeneity within the studied Cenomanian rock units will be evaluated.

Geologic setting

The north Western Desert of Egypt constitutes several petroliferous rift basins that were developed during the Mesozoic breakup of the Gondwana landmass and the birth of the southern Neo-Tethys (Garfunkel 1998, 2004; Guiraud et al. 2005; Tassy et al. 2015; Leila et al. 2022a). These basins are mostly aligned in a series of E-W, NE-SW, and ENE-WSW oriented half grabens (Fig. 1; Guiraud et al. 2005; Moustafa 2008; Bevan and Moustafa 2012). Besides the studied Abu Gharadig (AG) basin, they include Natrun, Shushan, and Matruh as well as Faghur-Siwa basins. The AG represents an intracratonic E-W-trending basin in the central northern part of the Western Desert (Fig. 1). The basin was actively subsiding since the Paleozoic with a down warping initiated in Carboniferous and continued until Early Cretaceous (Kitchka et al. 2015; El Gazzar et al. 2016; Sarhan 2017; El Mahdy et al. 2019). Similar to all the northern

basins of the Western Desert, Abu Gharadig is a part of the extensive Tethys passive margin that evolved during the Late Triassic-Jurassic crustal break-up of the Gondwana landmass (Guiraud 1998; Bosworth et al. 1999; Stampfli et al. 2001; Garfunkel 2004). Rift-related subsidence during the Jurassic permitted the accumulation of this syn-rift siliciclastics and mixed siliciclastics carbonate facies in all the north Western Desert basins (Ras Qattara, Khtataba and Masajid) (Fig. 2). The subsurface data from all the Western Desert rift basins suggest prevailing NW-SE extension tectonics during the initial opening phase (Longacre et al. 2007; Bevan and Moustafa 2012; Abdel Maksoud et al. 2018). This is confirmed on seismic profiles by a dominant pattern of NE-SW extensional faults (Fig. 3a, b). By the beginning of the Early Cretaceous, a clockwise rotation of the extension direction prevailed toward the NE-SW, thus resulting in a generation of complex fault patterns with continuous subsidence and deposition of Clastics-dominated Cretaceous sediments in Abu Gharadig Basin (Dolson et al. 2001; Bosworth et al. 2008; Ibrahim et al. 2009; Mousa et al. 2011).

The Jurassic-Cretaceous extensional phase was followed by a compressional episode during the Late Cretaceous and continued until the end of the Eocene due to the convergence between Africa and Eurasia (Guiraud and Bosworth 1997; Dolson et al. 2001; Guiraud et al. 2005; Bosworth et al. 2008; Bevan and Moustafa 2012). This convergence plate movement resulted in the structural inversions of the north Western Desert rift basins including Abu Gharadig and therefore inverted structural patterns extended as a foldbelt across the whole north Western Desert (e.g. Moustafa and Khalil 1990; Guiraud and Bosworth 1997). The studied seismic profiles document these inverted structural patterns which form excellent hydrocarbon traps (Fig. 3a, b). The Upper Cretaceous sedimentary successions consist mainly of mixed siliciclastics carbonate facies marked by fluvial to shallow-marine Kharita sediments at the base grading upward into shallow marine Clastics of the Bahariya Formation. These Clastics are overlaid by transgressive carbonate of the Abu Roash Formation (Abu Roash "G" Member). The Bahariya Formation and AR/G Member petrophysically have been studied by numerous authors such as Temraz et al. (2009), Abu Shady et al. (2010), Shazly and Nouh (2013), Abdel-Fattah et al. (2018), Farrag et al. (2021), Abu-Hashish and Said (2016), Tian et al. (2018), and Saleh et al. (2021).

Material and methods

Seismic data

The available seismic data include 2D seismic profiles covering an area of approximately 70 km² in the GPY field. Interpretation of seismic profiles included
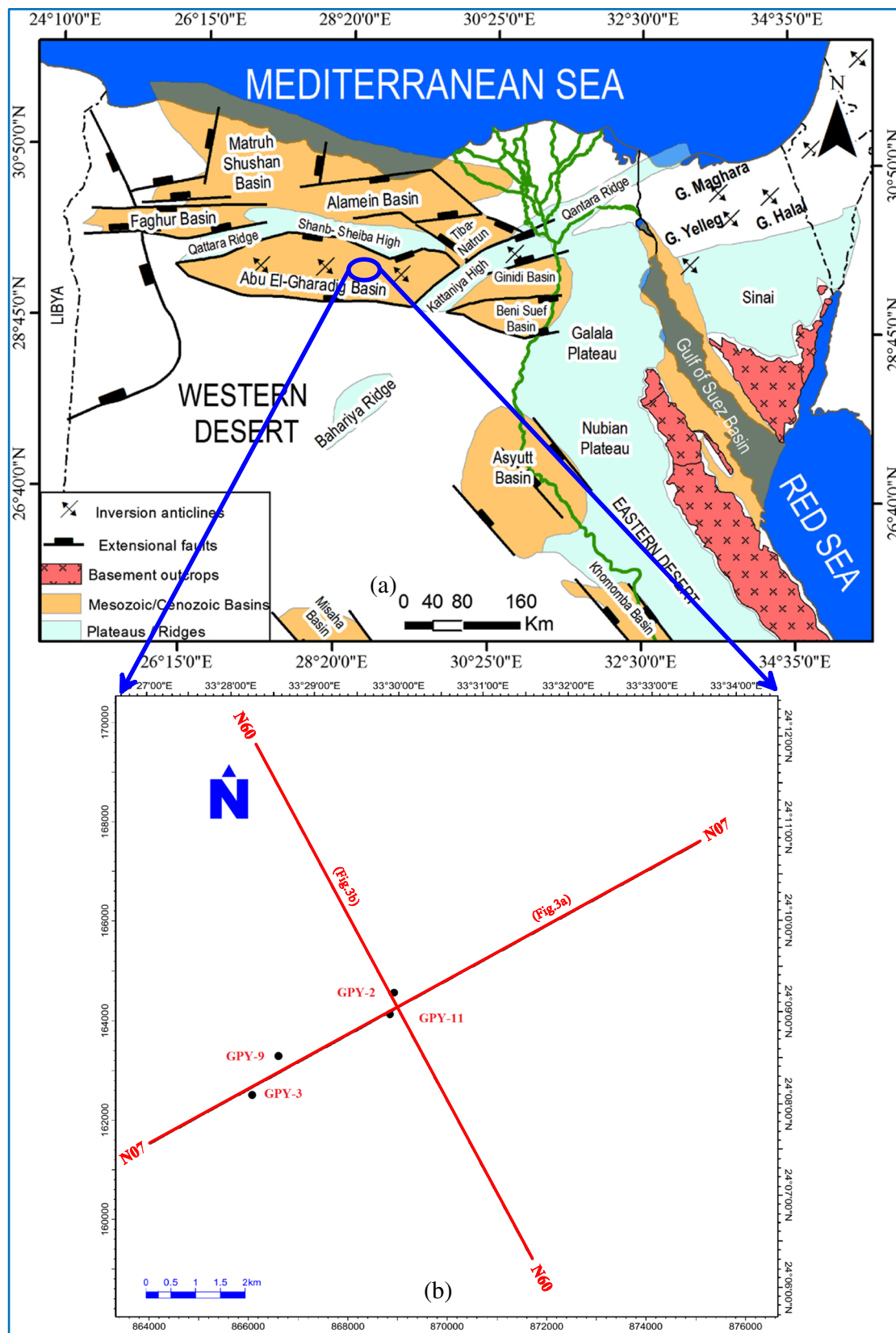
Fig. 1 A map illustrating the location of the GPY oil field wells in Abu Gharadig Basin, north Western Desert, Egypt (**a**) as well as the investigated 2D seismic lines (**b**)
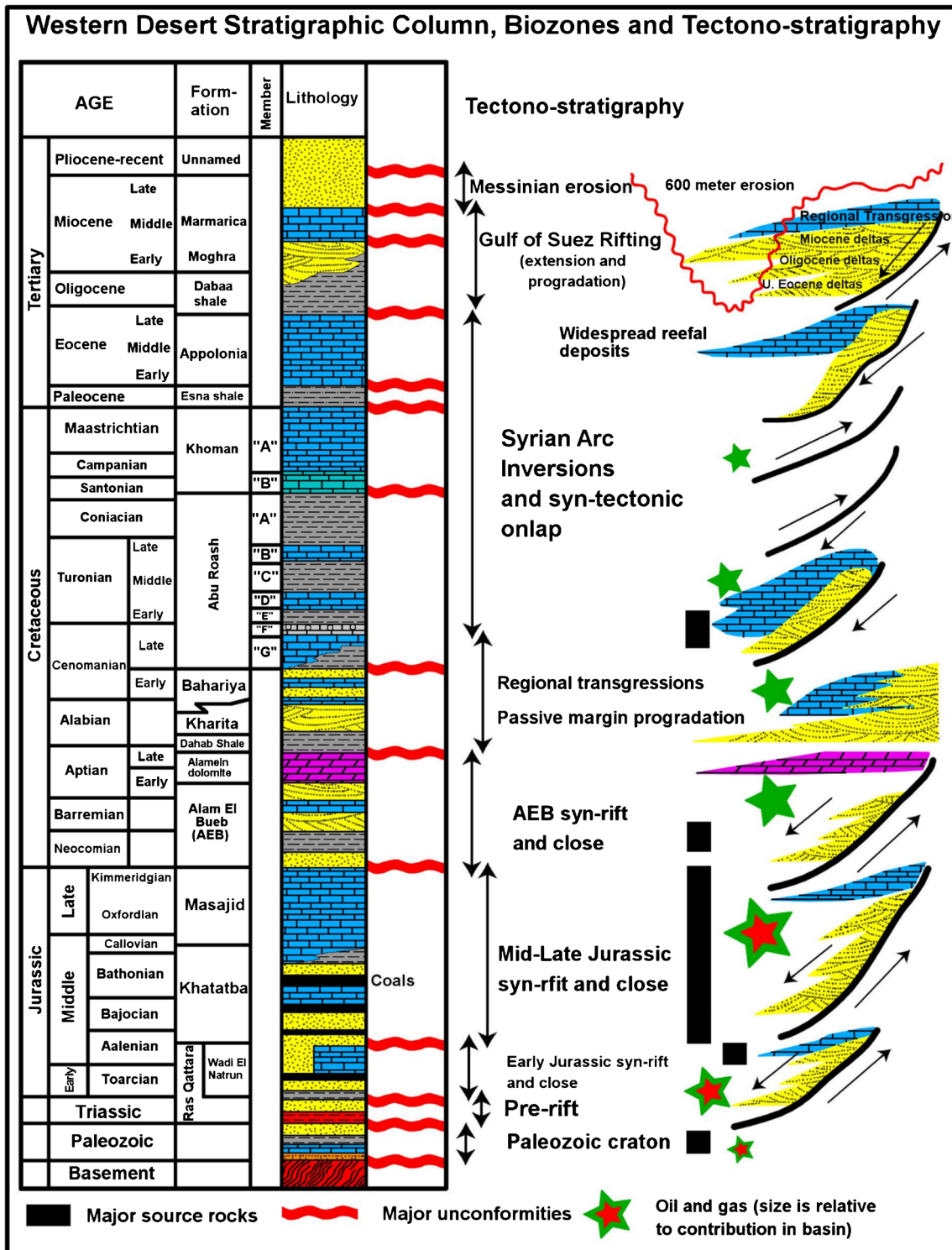
Fig. 2 Generalized stratigraphic column of the North Western Desert of Egypt (Schlumberger 1995; Wescott et al. 2011)

picking the main seismic-stratigraphic horizons (Bahariya, AR/G) and identification of the cross-cutting faults based on the discontinuities in seismic reflections (Abdel-Fattah et al. 2018; Henaish et al. 2022).

Moreover, structural contour maps of the top studied horizons were constructed on the picked surfaces. Different seismic facies within the studied horizons were interpreted based on their variation in some
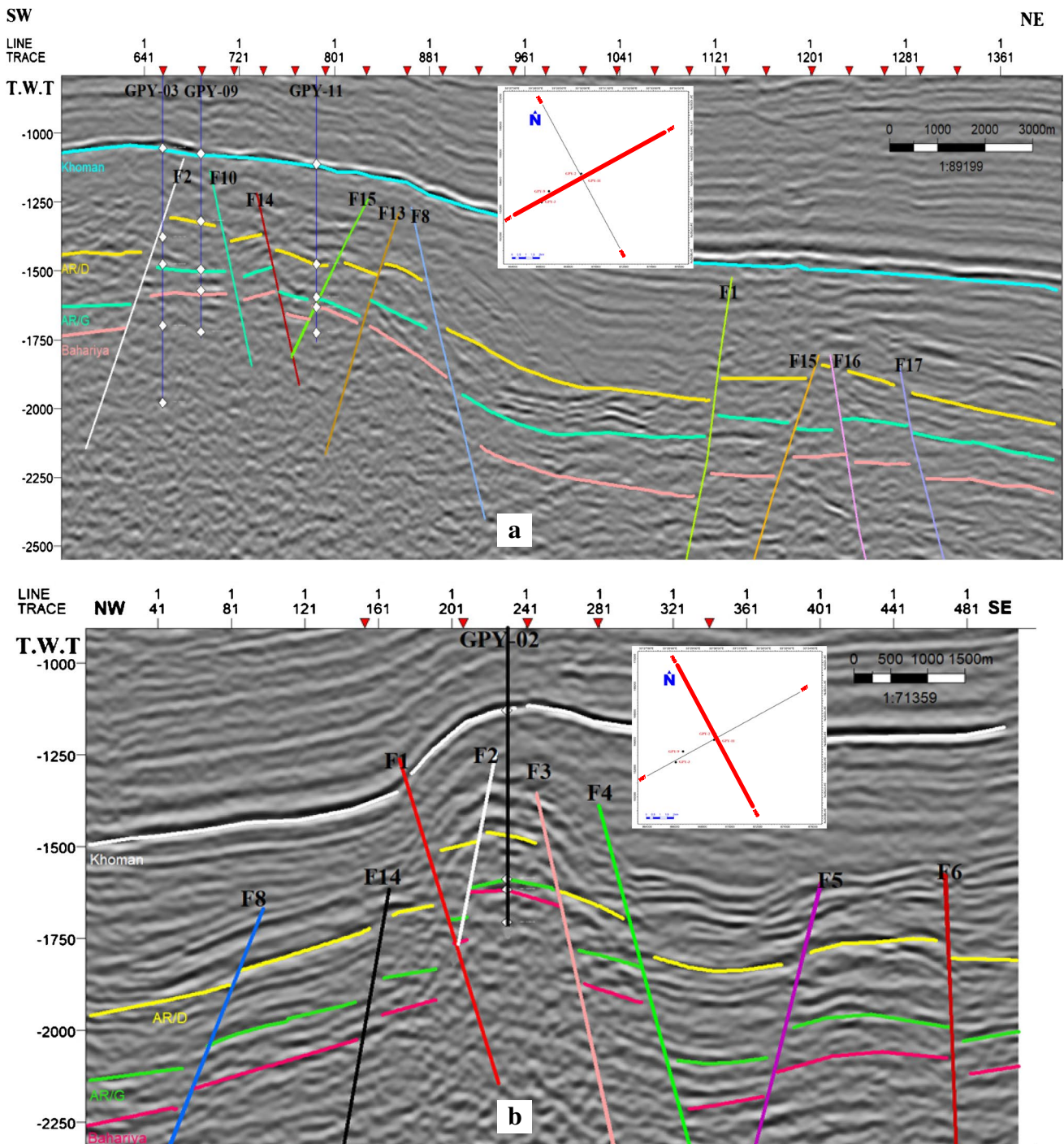
Fig. 3 Interpreted seismic profiles along strike (**a**) and dip (**b**) illustrating the dominant extensional structural patterns in the study region (Henaish et al. 2022)

specific seismic characteristics (e.g., seismic reflectivity, continuity, and amplitude) following the standard seismic stratigraphic procedure of Mitchum et al. (1977). Seismic data analysis allowed the identification of the structural patterns that affect the different

stratigraphic horizons. Variation in seismic characteristics (amplitude, reflectivity) was compared with well-data after performing seismic well-tie and permitted understanding variation in seismic facies with sedimentary patterns.

Wireline logging interpretation

Complete wireline log suites from four wells (GPY-2, GPY-3, GPY-9, and GPY-11) were utilized in this study. The available well logs comprise natural and spectral gamma ray "GR," "SGR," caliper "CAL," spontaneous potential "SP," compensated sonic "DT," formation density compensated logs "RHOB," and photoelectric factor effect (PEF). Additionally, neutron "CNL," deep Laterolog "LLD," shallow Laterolog "LLS," and micro spherical logs "MSFL" were also available for the studied wells. Prior to performing the calculations, adjustments were performed to reduce the influence of several factors on the well-log data, including lithology, mud weight, borehole temperature, and formation temperature. The petrophysical properties of the geological intervals of the Bahariya Formation and AR/G Member that may include highly promising hydrocarbon zones have been identified using the adjusted data. The well log analysis followed by potential reservoir petrophysical evaluation has been performed in a successive and interrelated sequence as follows: determination of formation temperature, determination of mud filtrate resistivity, and determination of shale volume (Vsh) (gamma-ray and neutron-density methods). Finally, the Calculation of the total ($\varnothing$t) and effective ($\varnothing$e) porosity depended on the using of neutron-density method (Fig. 4).

The available well logs were analyzed using Schlumberger Techlog 2015 software and the outputs were interpreted and presented in vertical lithosaturation cross-plot and isoparametric distribution maps. Different matrix cross plots were applied to differentiate between the main reservoir rock-forming lithologies and minerals such as sandstone, shales, and carbonate lithologies. In complex lithology, the (M-N) cross-plot or three-dimensional (3-D) cross-plot is often called litho-porosity cross-plots. The M and N parameters are derived using the readings of the neutron, sonic, and density logs together (Bruke et al. 1969; Schlumberger 1974). M and N are deduced as follows:

$$M = \frac{\Delta tfl - \Delta tlog}{\rho b - \rho fl} \times 0.01 \tag{1}$$

$$N = \frac{\varnothing Nfl - \varnothing Nlog}{\rho b - \rho fl} \tag{2}$$

where: Δtfl is the transit time of the saturation fluid, ρb density log reading, and ρfl fluid density; (ΦNfl) is the hydrogen index of the fluid and (ΦN) the neutron log reading. For saline mud Δtfl = 184 μ sec/ft, ρfl = 1.1 gm/cc, and ΦNfl = 100%.

Thin-bed analysis (TBA) is a suitable way to prove how various combinations of logs would respond to porosity, lithology, and shale type and content. Shale mineralogy and distribution were interpreted using a spectral gamma ray log. Thomas–Stieber analysis was utilized for the evaluation of

Fig. 4 A flow chart illustrates the sequence of different analytical approaches that were followed in this study for wireline logging data interpretation
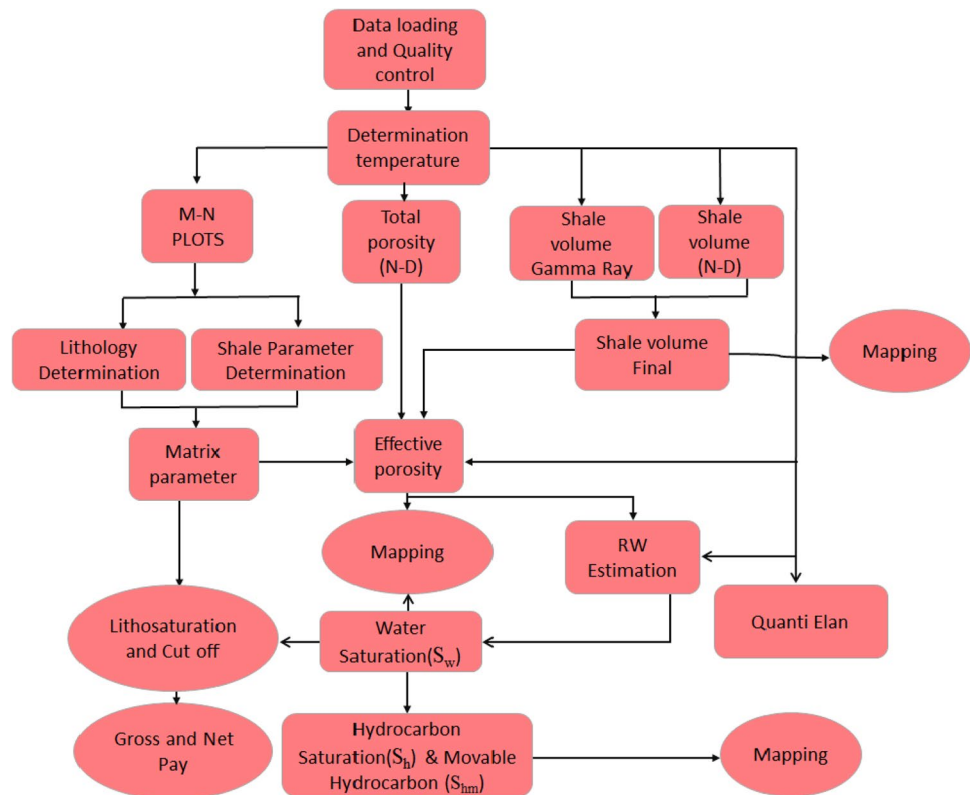
thin-bedded shaly-sand reservoirs, whose bed thicknesses are too thin to be resolved by traditional tools (Thomas and Stieber 1975). The parameters are derived using the total shale volume (Vsh) and total porosity ($\varnothing t$) of the shale determined using the gamma-ray and density logs. The shale and sand endpoints should be picked in different cross-plots. Thomas–Stieber method needs the total shale porosity and porosity of clean sand ($\varnothing ss = \varnothing max$). According to the method, the volume of laminar shale can be calculated by this formula:

$$Vlam = \frac{\varnothing t - \varnothing max + Vsh \times (1 - \varnothing sh)}{(1 - \varnothing max)}$$

Calculation of the volume of dispersed and structural shale can be obtained from these formulas (Thomas and Stieber 1975):

$V_{sh}\, str = Vsh - V\, lam$ For laminar-structural shale distribution.

$V_{sh}\, disp = Vsh - V\, lam$ For laminar-dispersed shale distribution.

Calculation of the total porosity ($\varnothing t$) and effective porosity ($\varnothing e$):

$$\varnothing tsand = \frac{\varnothing t - (Vlam \times \varnothing sh)}{(1 - Vlam)}$$

$$\varnothing esand = \frac{\varnothing t - (Vsh \times \varnothing sh)}{(1 - Vlam)}$$

Results and discussion

Seismic facies analysis

On seismic, the Bahariya Formation is characterized by vertically variable amplitude and frequency reflections. It comprises semi-parallel and discontinuous reflections. The Bahariya seismic reflections are partly chaotic and their amplitude decreases upward reflecting an upward variation in sedimentary facies and/or fluid content (Fig. 3a, b). On the other hand, AR/G seismic facies constitutes well-bedded, continuous, parallel, high amplitude, and reflectivity reflections. The AR/G seismic facies are vertically and laterally uniform in the study area reflecting its deposition during the same phase of sedimentation without significant variation either in lithology or fluid content (e.g., Mitchum et al. 1977; Leila 2019, 2022b). The depth structure contour map on the top of the Bahariya Formation shows an irregular distribution pattern with local structural highs in the central and western part of the study region (Fig. 5a). The structural highs are bounded by faults from all directions forming a perfect four dip-way closure structure (Henaish et al. 2022).
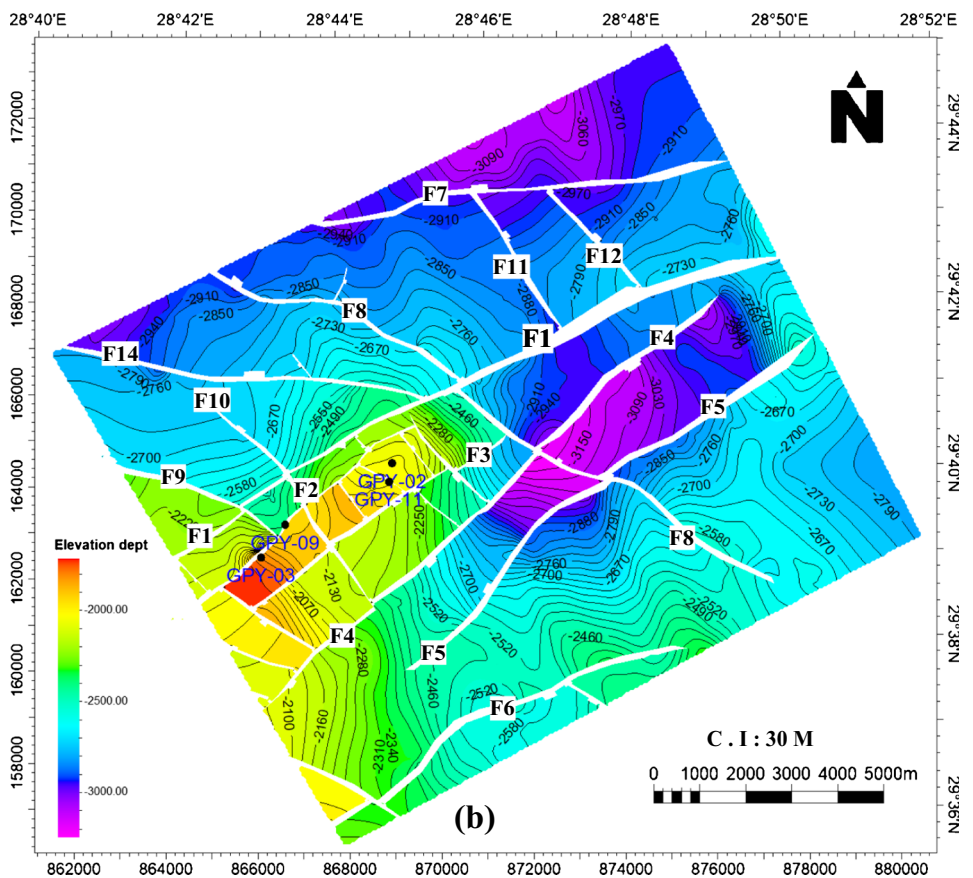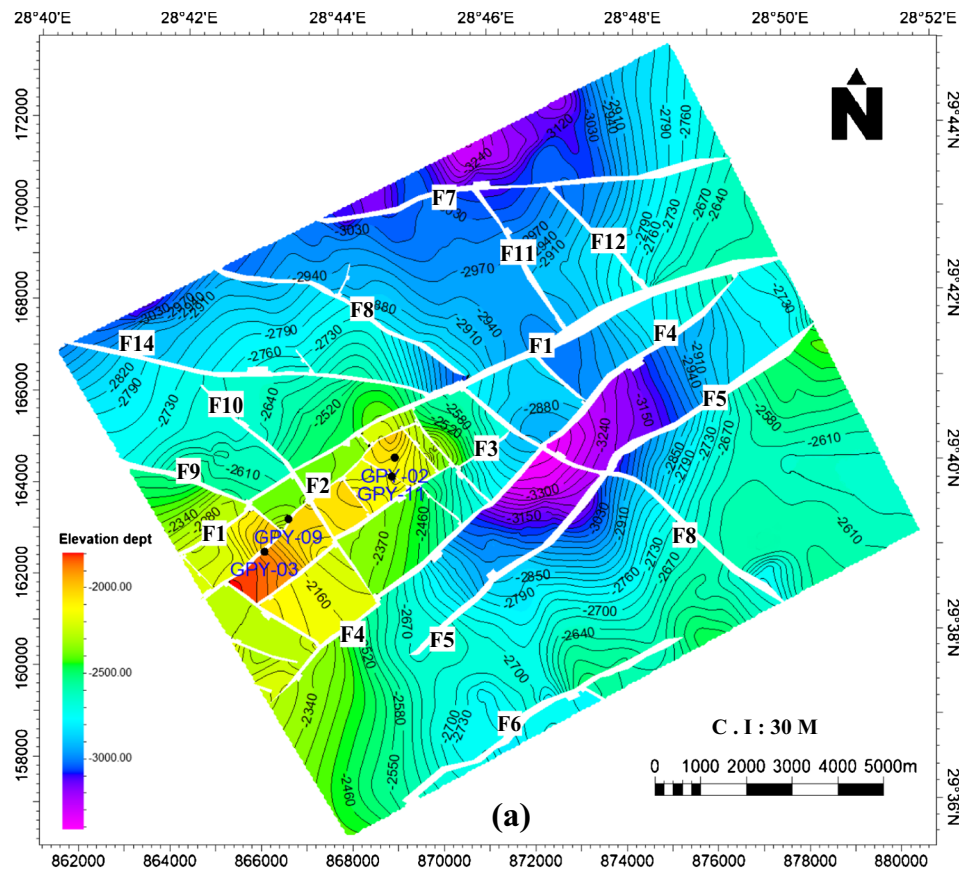
A similar pattern was also observed in the depth structure contour map on the top of the AR/G where the four dip-way closure structures also exist in the central and western part of the study area (Fig. 5b). This structure was formed contemporaneously with the late Cretaceous–Paleogene inversion phase due to the convergence between Africa and Eurasia (e.g., Mustafa and Khalil 1990; Guiraud and Bosworth 1997). This tectonic phase was likely responsible for the hydrocarbon trap formation in Abu Gharadig Basin.

Lithosaturation characteristics of Bahariya and AR/G sediments

The plotting of the caliper log with the bit size reveals that there is a huge washout in the four wells of the study area, which has a significant impact on the reading of the logs, particularly the neutron and density logs. We attempted to mitigate the impact of washout with applying all necessary correction on all the raw data before the final analysis. Based on vertical variation in lithological and petrophysical properties, the Bahariya Formation is identified into three different units. The lower Bahariya unit (B-3) is at the bottom, followed by the middle Bahariya unit (B-2), and the upper unit Bahariya unit (B-1) (Figs. 6, 7, 8, and 9). The B-3 unit consists mainly of sandstone and siltstone. The presence of carbonate minerals (limestone and dolomite) likely reflects their occurrence as pore-filling cement (e.g., Yasser et al. 2021). The occurrence of siderite, hematite, clay content, glauconite, and pyrite is indicated by low resistivity and high gamma-ray log readings (Mohamed et al. 2016). B-3 is characterized by an elevated shale volume due to the presence of siltstone. The highest effective porosity ($\varnothing e$) and hydrocarbon saturation (S_h) values of 17% and 69% for B-3 in the GPY-2 well are reported between 2321 and 2324 m (Fig. 6). B-3 unit is comparatively sand-rich in GPY-3 with the highest $\varnothing e$ and S_h values of 43% and 83%, respectively (Fig. 7). Therefore, the highest net pay thickness is reported in GPY-3 well. On the other hand, B-3 unit is dominated by siltstone with thin sandstone interbeds in GPY-9 and GPY-11 wells and therefore display comparatively lower $\varnothing e$ and S_h values (Figs. 8 and 9).

The B-2 unit is dominated by sandstone and siltstone with thin shale interbeds. In GPY-2 well, the highest $\varnothing e$ and S_h values are respectively 23% and 93% where hydrocarbon-bearing pay zones are observed in this unit between 2265–2277 m and 2295–2300. In GPY-3 well, the $\varnothing e$ and S_h values are comparatively lower (17%, and 64%, respectively) where the facies are more clay-rich. Moreover, in the GPY-9 well, the highest $\varnothing e$ and S_h values are 21% and 54%, respectively, where a 1-m thick streak of hydrocarbon pay zone is reported at 2309–2310 m. Similarly, GPY-11 well constitutes only a 1.5-m thick pay zone (2294–2295.5 m) in B-2 unit with average $\varnothing e$ and S_h values of 31% and 64%.

Fig. 5 Depth structural contour map on the top of Bahariya Formation (**a**), and Abu Roash G (AR/G) member (**b**) in GPY oil vicinity in Abu Sennan Concession, Western Desert, Egypt (Henaish et al. 2022 and Farrag et al. 2022)
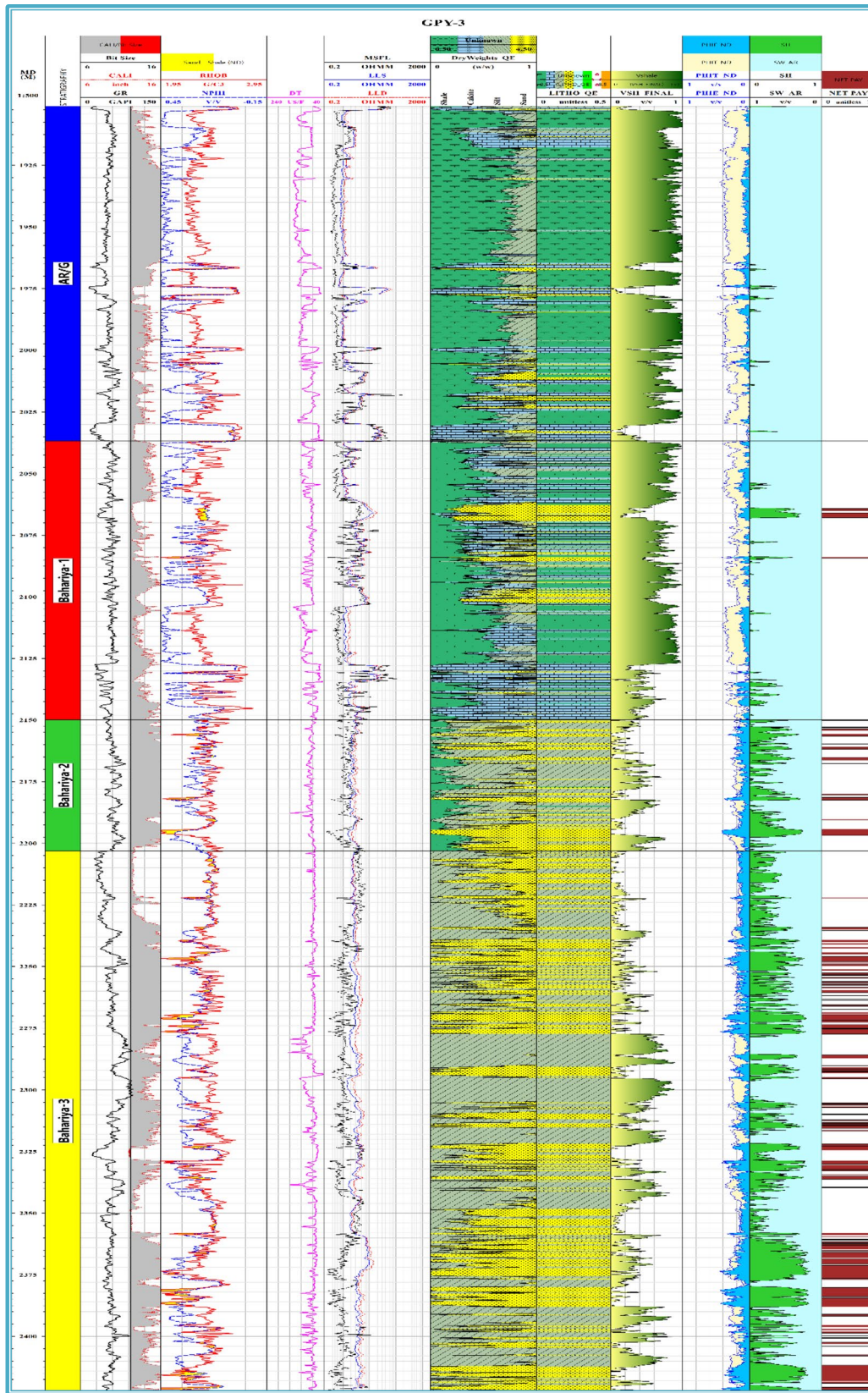
Fig. 6 Vertical litho-saturation cross plot showing the lithologic and petrophysical properties of the studied rock units in GPY-2 well in GPY oil vicinity in Abu Sennan Concession, Western Desert, Egypt

Fig. 7 Vertical litho-saturation cross plot showing the lithologic and petrophysical properties of the studied rock units in GPY-3 well in GPY oil vicinity in Abu Sennan Concession, Western Desert, Egypt
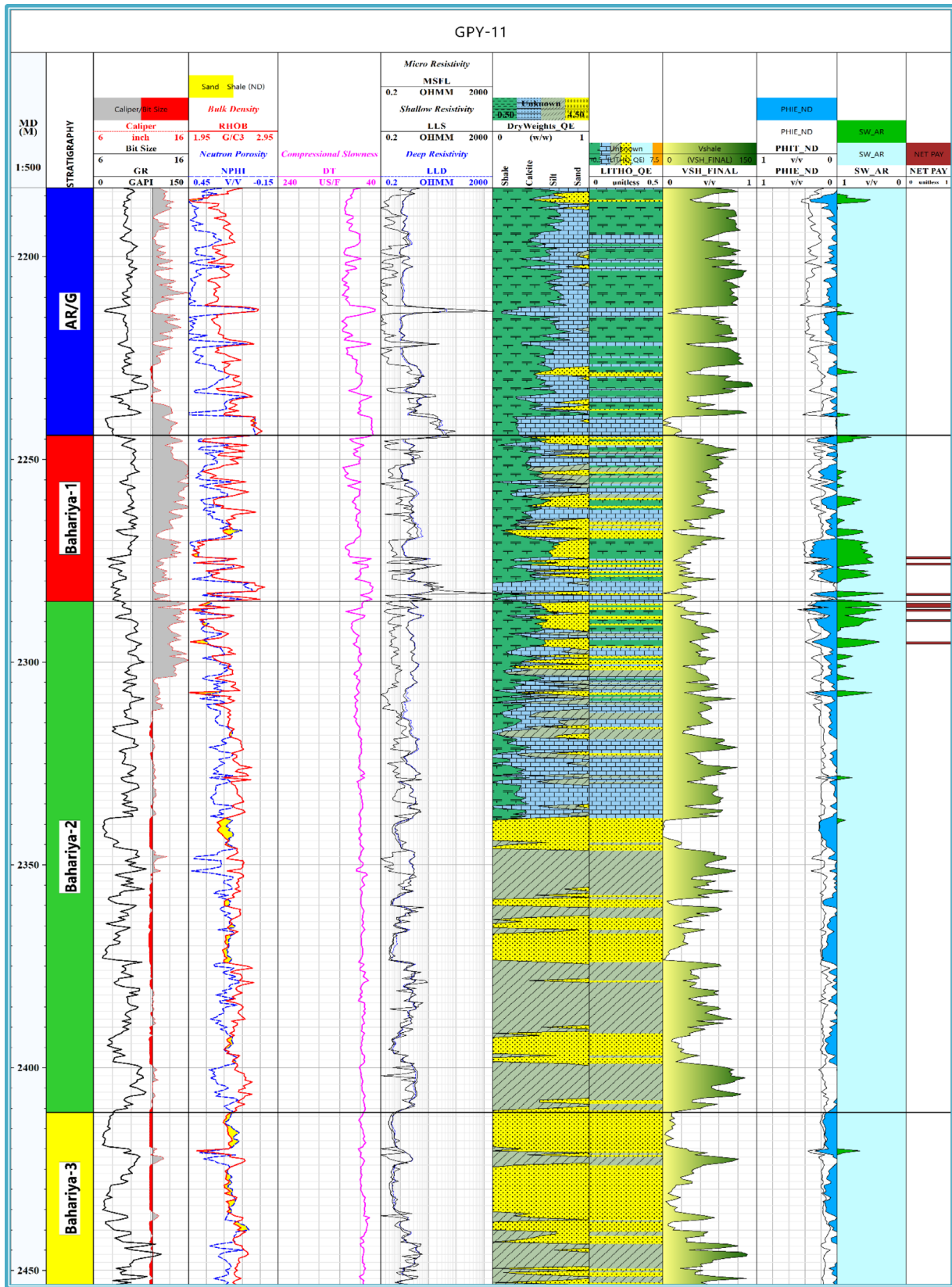
Fig. 8 Vertical litho-saturation cross plot showing the lithologic and petrophysical properties of the studied rock units in GPY-9 well in GPY oil vicinity in Abu Sennan Concession, Western Desert, Egypt

Fig. 9 Vertical litho-saturation cross plot showing the lithologic and petrophysical properties of the studied rock units in GPY-11 well in GPY oil vicinity in Abu Sennan Concession, Western Desert, Egypt

The B-1 unit is composed primarily of carbonate (limestone and dolomite), shale, and sandstone. In the GPY-2 well, the greatest $\varnothing_e$ and Sh values of 37% and 65% are observed between 2226 and 2231.5 m which is the main pay zone in the B-1 unit. In GPY-3, the maximum $\varnothing_e$ and S_h values are 17% and 64% in the 4-m thick pay zone identified between 2063 and 2067.5 m. The lowest value of S_h is reported for B-1 unit in GPY-9 and GPY-11 wells where no pay zones were observed in B-1 unit in these wells.

AR/G Member consists mainly of shale, limestone, dolomite, and sandstone with a very low content of siltstone. AR/G Member has the maximum $\varnothing_e$ and Sh values of 37% and 60% in the GPY-2. Hydrocarbon-bearing pay zones within AR/G Member are only reported in the GPY-2 well. In the other wells, AR/G Member is dominated by calcareous shale beds with very low $\varnothing_e$ values < 10%. Therefore, reservoir intervals are completely absent in AR/G Member in most of the studied wells.

Petrophysical parameters distribution

The different petrophysical parameters deduced from wireline logging interpretation for the Bahariya Formation units (B-3, B-2, B-1) as well as AR/G Member were mapped to define lateral changes and distribution of the best reservoir facies (Table 1). The mapped petrophysical parameters comprise shale volume (V_{sh}), effective porosity ($\varnothing_e$), movable hydrocarbon saturation (S_{hm}), and the net-pay thickness.

For the B-3 unit, the V_{sh} increases northward with a maximum value of 25% in the GPY-9 well and decreases in the southwest direction with a minimum content of 12% in

the GPY-3 well (Fig. 10a). The $\varnothing_e$ increases in the southwest direction with the highest effective porosity value of 27% in the GPY-9 well. It gradually decreases northeast with the lowest value of 13% in GPY-11 (Fig. 10a). The sediments of the B-3 unit are fully saturated with water in the eastern parts of the study area where the lowest content of movable hydrocarbon was reported (Fig. 10a). On the other hand, the movable hydrocarbon content increases in the northeastern and southwestern parts of the study region consistent with the occurrence of hydrocarbon pay zones in GPY-2 and GPY-3 wells. Figure 10b illustrates that the V_{sh} of the B-2 unit increases in the northwest directions, recording a maximum value of 31% through the GPY-9 well. It decreases in the southwest direction, reflecting a minimum shale content of 5% in the GPY-3 well. The $\varnothing_e$ recorded an overall increase in the south and east directions with the highest percentage of 32% in the GPY-11 well. It gains the lowest connected pore percent of 20% in GPY-2 (Fig. 10b). The S_{hm} recorded a maximum saturation of 41% through the GPY-2 well in the northeastern parts. This saturation decreases toward the northwestern direction recording an average value of 18% in the GPY-9 well (Fig. 10b). Finally, the thickness of the net pays intervals of nearly 24 m was recorded in the GPY-2 well and decreases to reach 0.3 m at the GPY-9 well (Table 1).

The V_{sh} of the B-1 unit increased in the northeast and southwest directions, recording a maximum volume of 27% through the GPY-3 well. It decreases in the northwest direction, reflecting a minimum shale volume of 3% in the GPY-9 well (Fig. 10c). The $\varnothing_e$ displays a general increase in the central part of the study region

Table 1 The values of petrophysical parameters for Abu Roash G member and the three units of Bahariya Formation for the studied wells in GPY oil and gas vicinity in Abu Sennan Concession, Western Desert, Egypt

FM	Units	Well	Gross thickness (m)	Vsh (%)	PHIE, (%)	S_w, (%)	S_h, (%)	S_{hm}, (%)	Net pay (m)
ABU ROASH FM	AR/G	GPY-3	135.8	0.32	0.07	0.43	0.57	0.16	0.2
		GPY-9	131.9	0.32	0.12	0.97	0.03	0.10	0.0
		GPY-11	61.0	0.36	0.14	0.83	0.17	0.14	0.0
		GPY-2	47.5	0.31	0.31	0.42	0.58	0.32	5.3
BAHARIYA FM	B-1	GPY-3	113.3	0.27	0.17	0.39	0.61	0.24	3.3
		GPY-9	87.0	0.03	0.32	0.38	0.62	0.12	0.5
		GPY-11	41.0	0.18	0.31	0.43	0.57	0.17	1.5
		GPY-2	30.4	0.26	0.25	0.41	0.59	0.37	7.8
	B-2	GPY-3	53.0	0.05	0.28	0.37	0.63	0.30	8.5
		GPY-9	95.0	0.31	0.28	0.46	0.54	0.18	0.3
		GPY-11	126.0	0.22	0.32	0.40	0.60	0.24	2.5
		GPY-2	49.0	0.17	0.20	0.25	0.75	0.41	23.9
	B-3	GPY-3	218.9	0.12	0.25	0.32	0.68	0.38	69.8
		GPY-9	77.5	0.25	0.27	0.41	0.59	0.19	1.1
		GPY-11	42.5	0.16	0.13	0.99	0.02	0.00	0.0
		GPY-2	78.6	0.23	0.17	0.37	0.63	0.28	3.5

Fig. 10 Petrophysical parameters distribution charts of shale volume, effective porosity, and movable hydrocarbon saturation in **a** Bahariya-3 unit, **b** Bahariya-2 unit, **c** Bahariya-1 unit, and **d** AR/G Member, GPY oil vicinity, Western Desert, Egypt
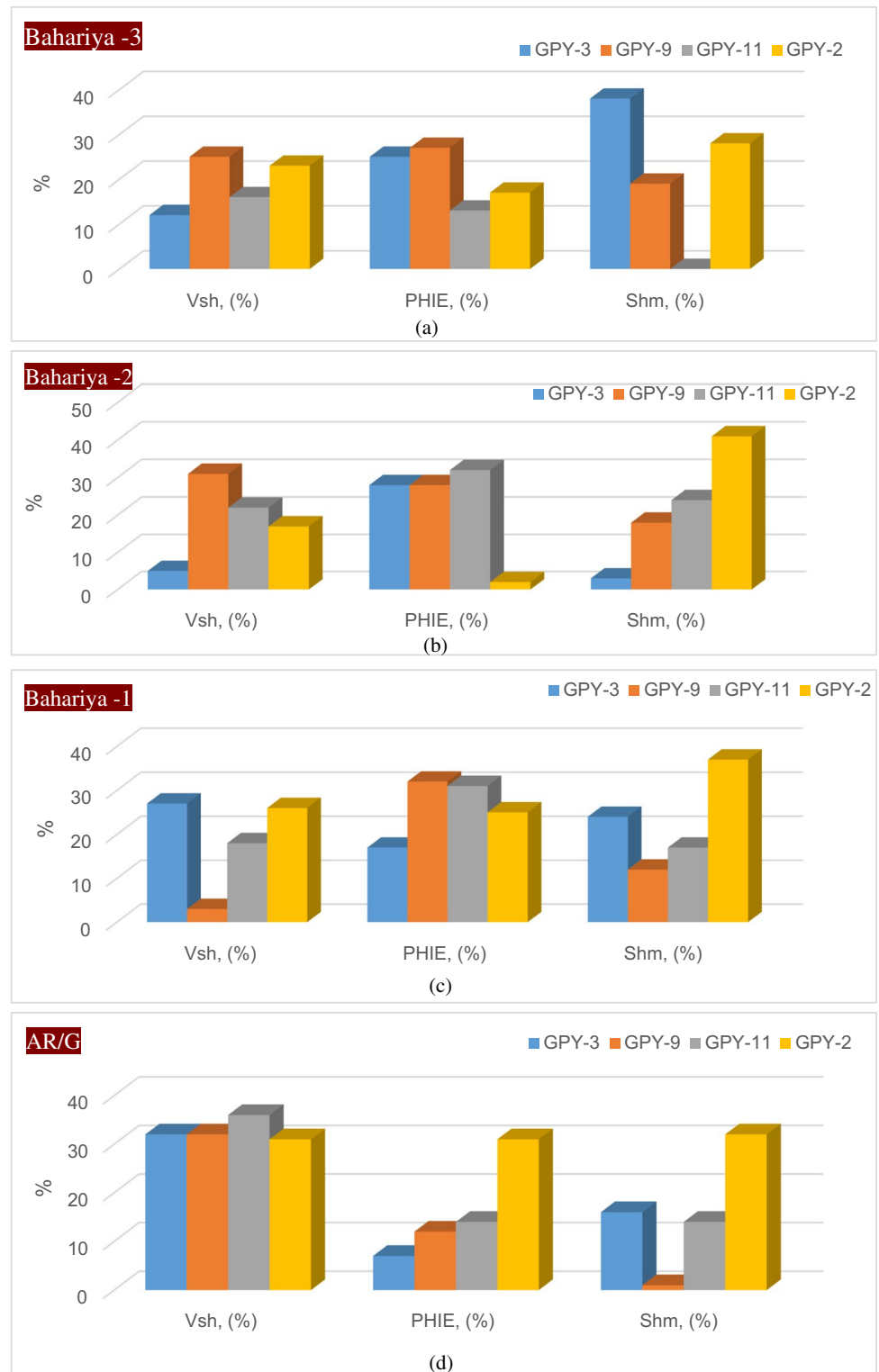
where the highest values of 32% are reported in GPY-9 and GPY-11 wells. It gradually decreases in the southwest direction with the lowest connected pore percent of 17% in GPY-3 (Fig. 10c). The S_{hm} recorded a maximum saturation of 37% through the GPY-2 well in the northeastern direction. This saturation decreases toward the northwestern direction recording 12% in the GPY-9 well (Fig. 10c). A maximum net pays interval of nearly 7.8 m was recorded in the GPY-2 well and it decreased to reach 0.5 m at the GPY-9 well (Table 1).

The V_{sh} of AR/G Member increased in the east direction, recording a maximum value of 36% through the GPY-11 well. It decreases in the north, southwest, and west directions, reflecting a minimum shale content of 31% in the GPY-2 well (Fig. 10d). The $\varnothing e$ recorded a general increase in the northeast direction with the highest effective porosity of 31% in the GPY-2 well. It regularly decreases in the southwest direction with the lowest connected pore percent of 7% in GPY-3 (Fig. 10d). The S_{hm} recorded a maximum saturation of 32% through GPY-2 well in the northeastern parts. This saturation decreases toward the northwestern direction recording an average value of 10% in the GPY-9 well (Fig. 10d). The maximum net pay intervals of nearly 5.3 m were recorded in the GPY-2 well and decrease to reach zero at GPY-9 and GPY-11 wells (Table 1). According to the distribution patterns of Cenomanian petrophysical characteristics, the GPY field's B-3 unit has a highly promising southwestern hydrocarbon potentiality, whereas the B-2, B-1 units, and AR/G Member all have northeastern high potentialities.

Reservoir lateral connectivity

Tracking both lateral and vertical variation in the architecture and distribution of reservoir sand bodies is crucial for hydrocarbon exploration and development strategies.

These variations are often dependent on the depositional setting which control the sedimentary stacking patterns (Posamentier and Allen 1999; Nabawy and El Sharawy 2015; Leila et al. 2022b). Stratigraphic architecture, sand-body geometry, and proportion of clay and fine materials are important factors to have an impact on reservoir facies connectivity (Tearpock and Bischke 1991; Bridge and Mackey 1993; Li et al. 2004; Colombera et al. 2016). The NE-SW stratigraphic cross-section passing through the studied wells shows wide variations in the thicknesses and lithological characteristics of the studied rock units (Fig. 11). For example, Bahariya unit 3 thickness in the southwest direction in GPY-3 well, however, the highest content of Bahariya unit 3 sand is observed in the northeastern part of the field where the thickness of Bahariya unit 3 (B-3) decreases. Despite the great thickness of Bahariya unit 3 in the GPY-3 well, the sand beds are thin, disconnected, and heterogeneous. The thickness of Bahariya unit 3 sandstone bodies is structurally rather than depositionally controlled. The inversion of the fault slipping during Late Cretaceous–Middle Eocene affected the NE-SW normal faults, which suffered positive structural inversion forming a symmetrical anticline with variated thickness distribution in the four Cenomanian units with the thicker interval on the hanging wall of these faults that extended throughout the study area of GPY oil field. The
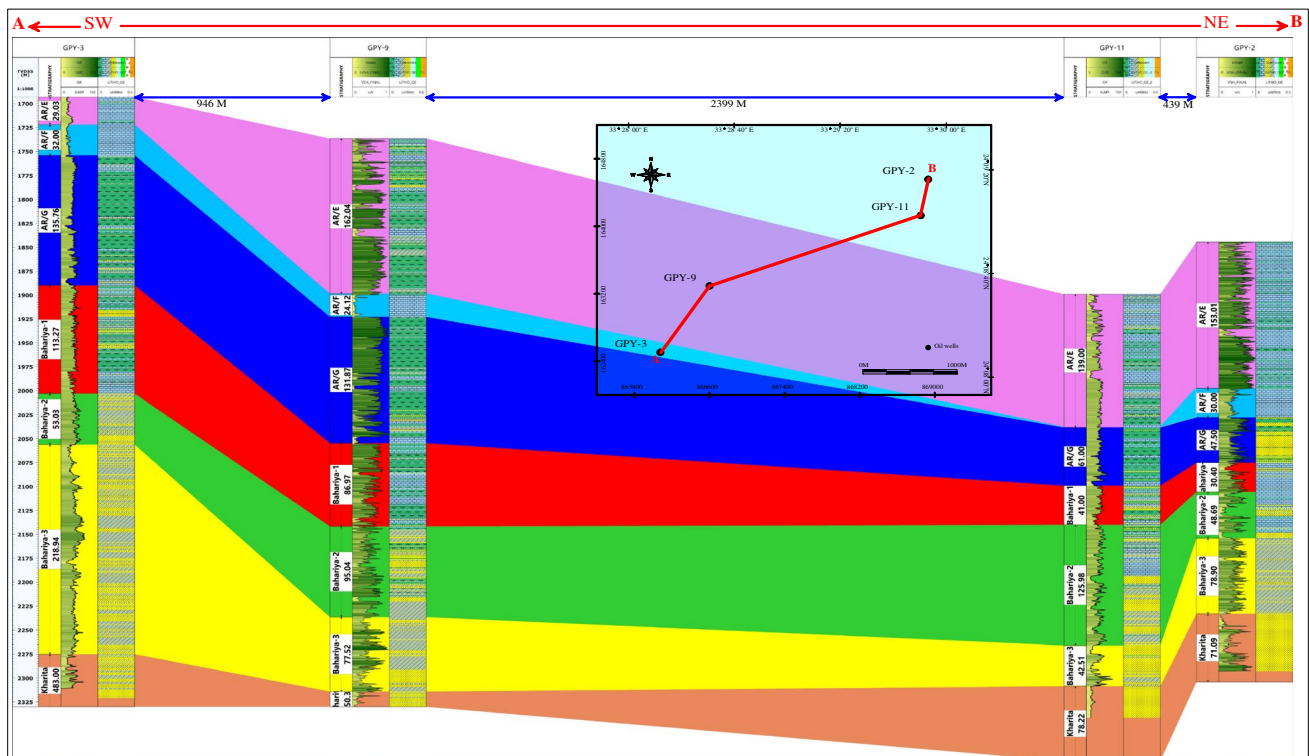

Fig. 11 Vertical litho saturation cross-plot correlation chart of the petrophysical parameters of Abu Roash G member and the three units of Bahariya Formation for the studied wells in GPY oil vicinity in Abu Sennan Concession, Western Desert, Egypt
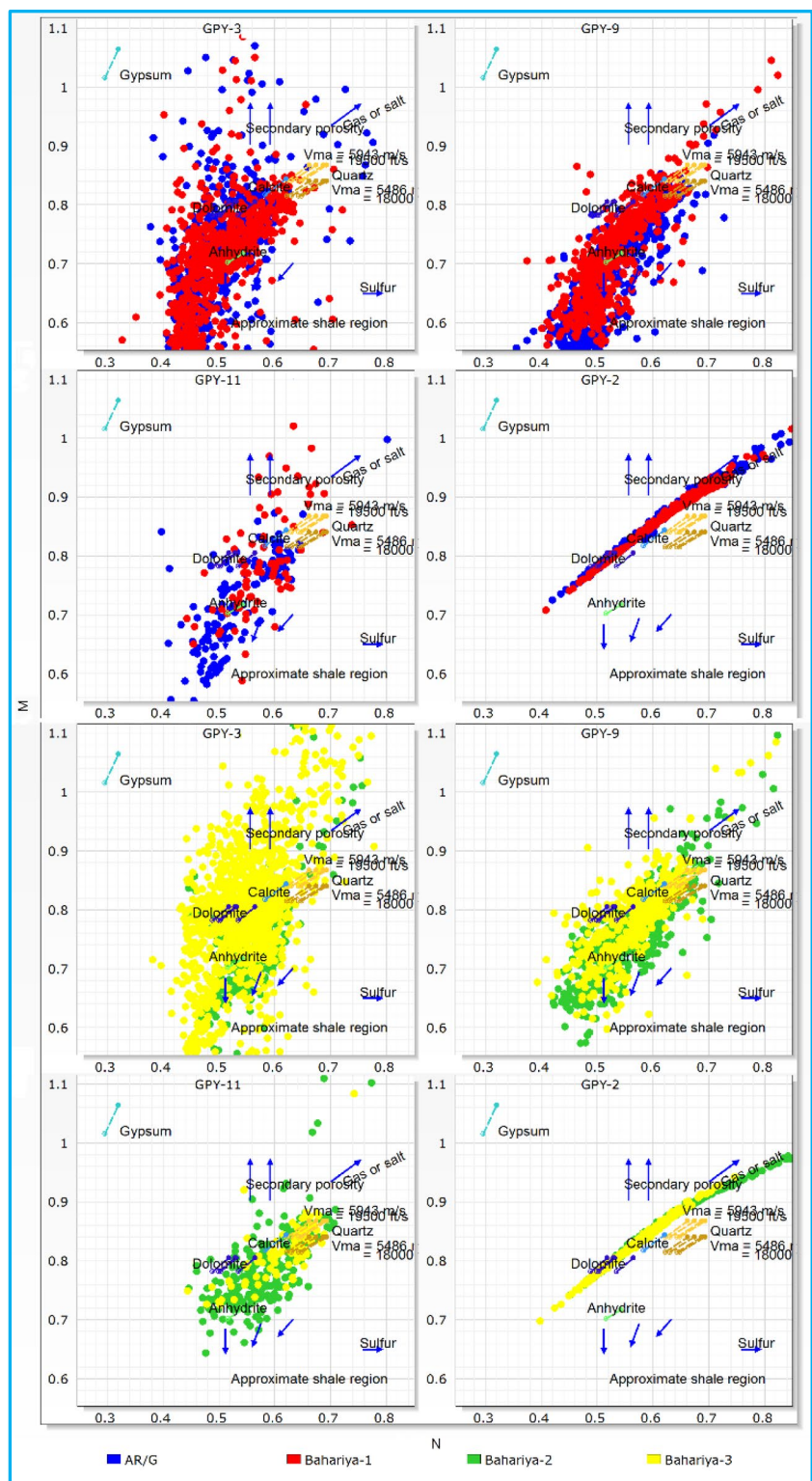
Fig. 12 Neutron-density cross plot of Abu Roash G member and the three units of Bahariya Formation for the studied wells in GPY oil and gas vicinity in Abu Sennan Concession, Western Desert, Egypt
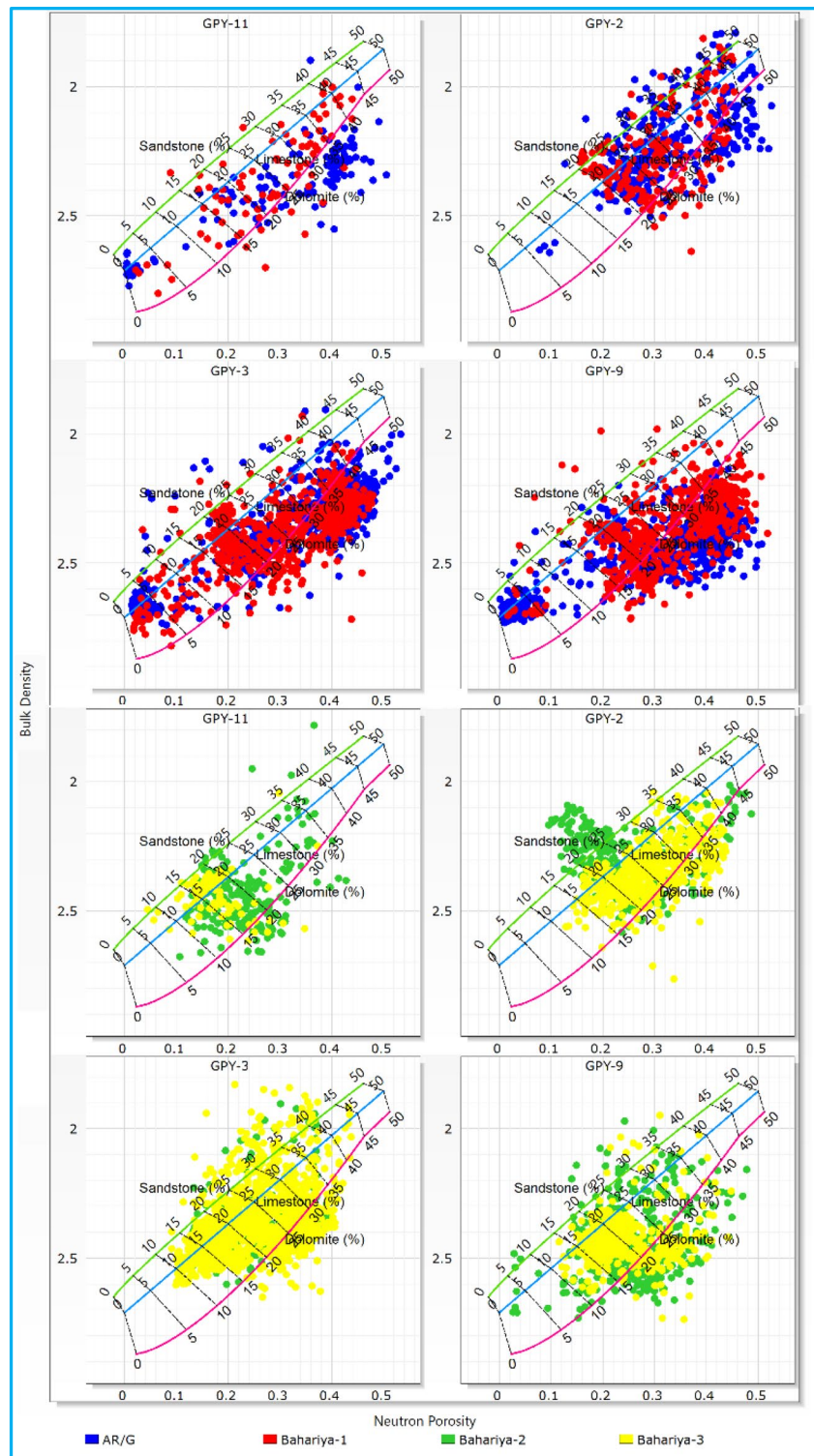
stratigraphic cross-section also reveals a lateral and vertical variation in the depositional facies from shallow to deep marine, where a shallow marine environment was reflected throughout the B-3 unit and extended along the study area. The B-2 unit represented shallow marine environments in the southwestern part and deep in the northeastern part, where the beginning of limestone deposition. The B-1 unit and AR/G Member are represented by deep marine environments. These fluctuating sediments affected greatly the petrophysical properties of the four Cenomanian horizons, especially the shale quantity, distribution as well as the porosity, permeability, and hydrocarbon potentiality.

Fig. 13 M-N cross plot of Abu
Roash G member and the three
units of Bahariya Formation
for the studied wells in GPY oil
and gas vicinity in Abu Sennan
Concession, Western Desert,
Egypt

Reservoir matrix analysis

The neutron-density cross-plot of the B-3 unit reflects in
dominant sandstone composition with limestone and shale
interbeds (Fig. 12). The sandstone porosity ranges from 20

to 25%. Limestone likely occurs as calcareous cement and
bed intercalations in the sandstones (Abdel Maksoud et al.
2019; Yasser et al. 2021; Leila et al. 2022a, b). The matrix
composition of Bahariya unit-2 (B-2) indicates a compara-
tively lower sand content than that in B-3. B-3 matrix is

Fig. 14 a PEF-density cross plot. **b** Thorium/potassium ratio — PEF cross plot. **c** Potassium% — PEF cross plot. **d** Potassium — thorium cross plot of Abu Roash G member and the three units of Bahariya Formation in GPY-9 well in GPY oil vicinity in Abu Sennan Concession, Western Desert, Egypt
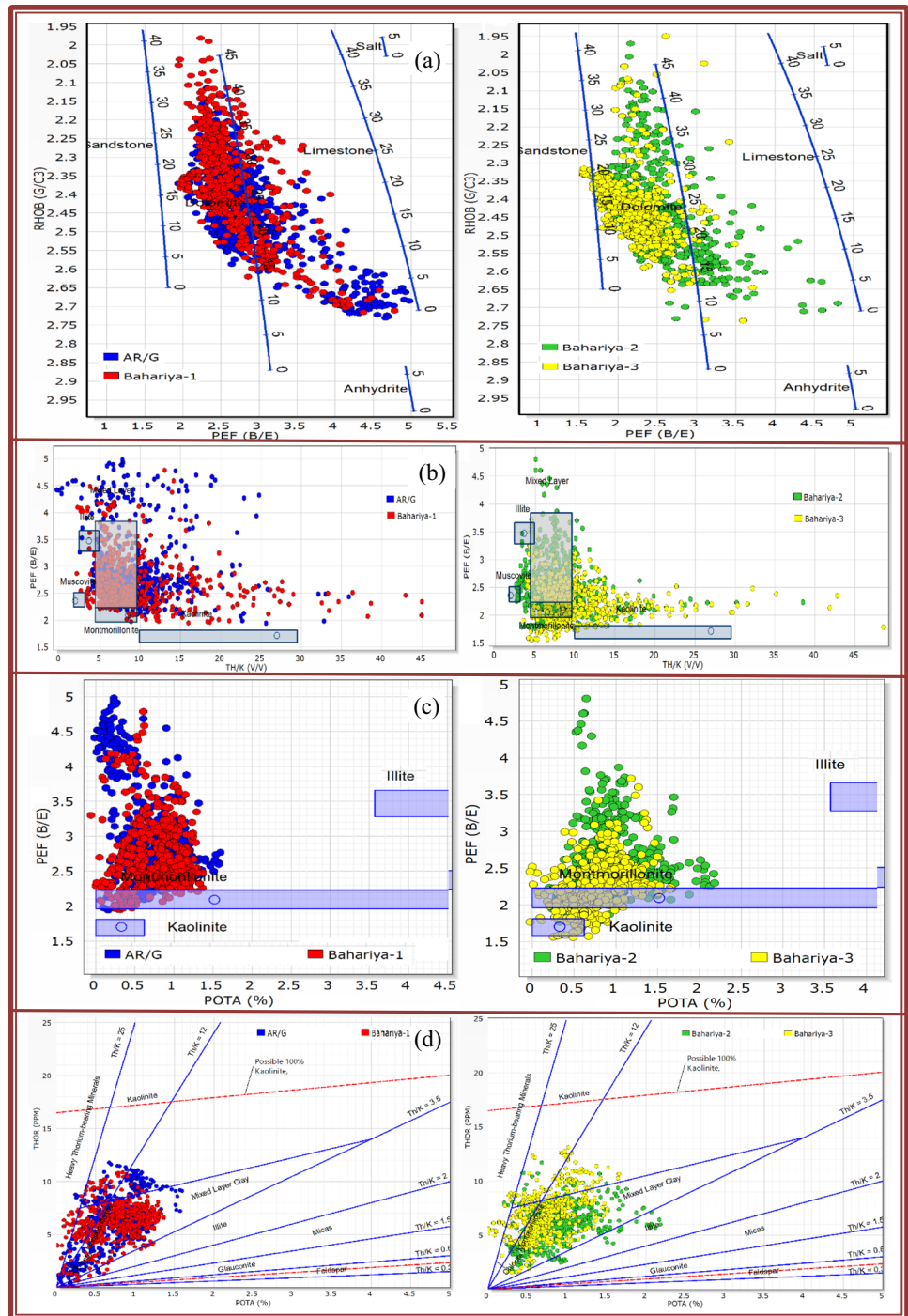

rather dominated by dolomite and limestone with sub-ordinate contents of siltstone and shale (Fig. 12). Bahariya-1 unit (B-1) matrix consists mainly of limestone with porosity values of approximately 15%. Similar to B-1, the matrix composition of AR/G is dominated by limestone and shale with rare sandstone and siltstone contents (Fig. 12). Matrix analysis of the Cenomanian sedimentary facies in GPY Field reveals an upward increase in the shale and carbonate content and a decrease in the sand content confirming a

transgressive depositional phase that prevailed in the study region during Late Cenomanian. This transgressive phase was likely accompanied by a prominent change in the depositional facies from fluvial-dominated (B-3) at the base to shallow and deep-marine deposition at the top (B-3 and AR/G) (Leila et al. 2022b).

M-N cross-plot allows the identification of the dominant mineralogical composition of the studied Cenomanian rock units. The plot shows that B-3 unit sediments are

Fig. 15 Gamma ray-density and neutron-density cross plots of the sandstone of **a** B-3 unit, **b** B-2 unit, **c** B-1 unit, and **d** Abu Roash G member in GPY oil vicinity in Abu Sennan Concession, Western Desert, Egypt
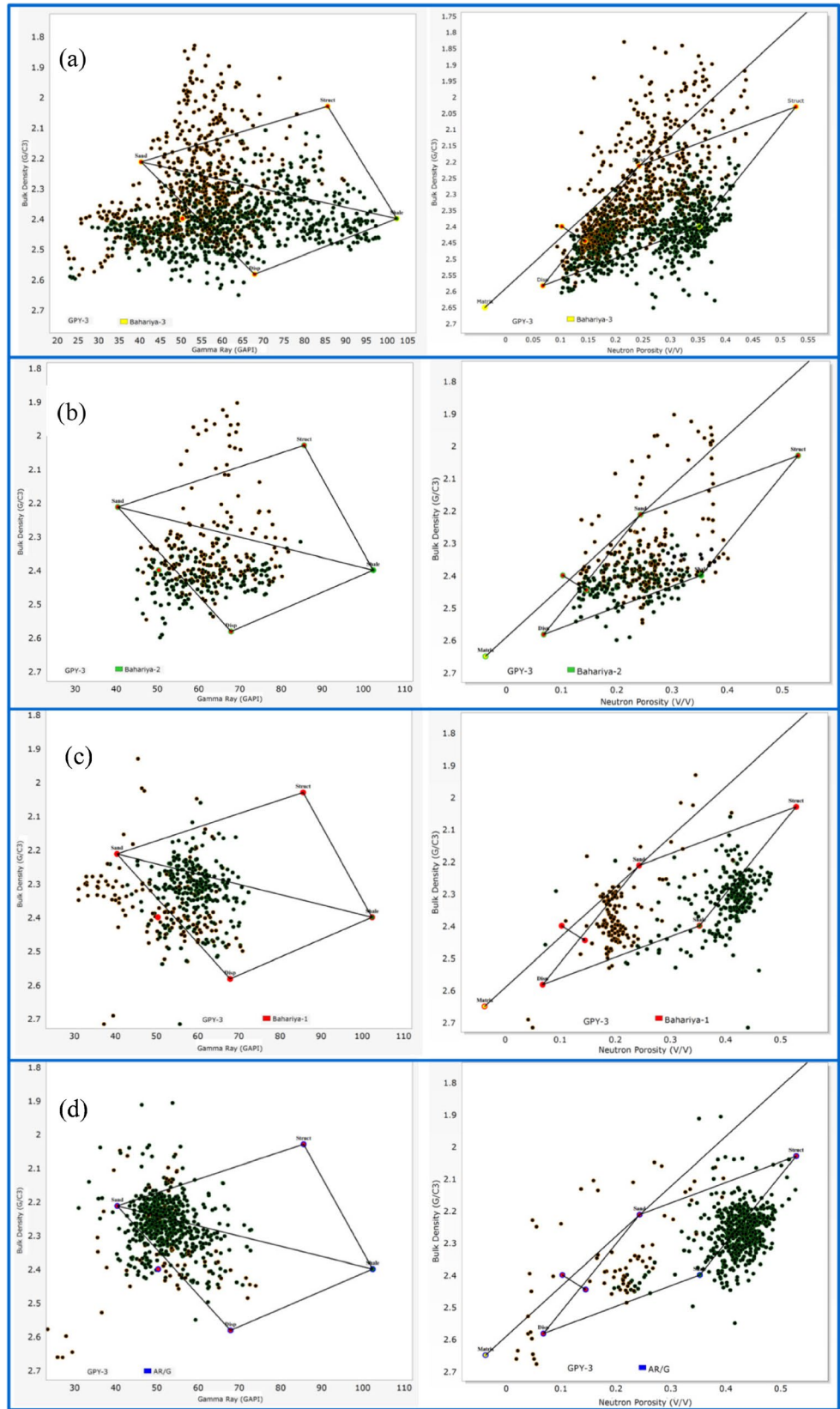
preliminary and consist of quartz and calcite with subordinate content of clay minerals (Fig. 13). B-3 sediments also contain significant volumes of secondary pores evidenced by shifting of the B-3 points upwards. Secondary porosity in B-3 sandstones suggests a prominent dissolution of the calcite cement and/or the calcareous clasts (e.g., Radwan et al. 2022). B-2 sediments contain less content of quartz and their mineralogical composition is dominated by calcite and clay minerals. Secondary porosity is less common in B-2 compared with B-3 typifying a mild extent of dissolution and the carbonate materials mostly occur as concretions in the sand and thin-bed intercalations. Shale is the main lithology in the B-1 unit and its sediments mainly consist of clay minerals and carbonate. Similarly, AR/G facies are dominated by calcite, dolomite, and clay minerals, and the effect of secondary porosity is observed in some wells. Secondary porosity is mostly attributed to the dissolution of carbonate components.

The photoelectric factor (PEF) versus bulk density (RHOB) cross plot confirms the dominant quartzose sandstone composition of the B-3 unit and the mixed siliciclastics-carbonate composition of the other units (Fig. 14a). Such upward transitions from Clastics-dominated sedimentation in B-3 into mixed siliciclastics-carbonate upward confirm a major change in the depositional environment during the Cenomanian with increasing the marine influence during Late Cenomanian (e.g., Hantar 1990; Helba and Bakry 1996; Alsharhan and Abd El-Gawad 2008; Leila et al. 2022b).

Clay mineral identification

The occurrence of clay minerals in the reservoir is often crucial for reservoir management as they induce a major influence on the reservoir storage and flow capacities (e.g., Walderhaug et al. 2012; Leila and Mohamed 2020; El Adl et al. 2021). Moreover, physical and chemical characteristics as well as the performance of conventional sandstone, carbonate, and unconventional shale are significantly influenced by the presence of clay minerals (e.g., Schon 2011; Jiang 2012; Chou et al. 2014). Migration of fines and swelling of specific clay mineral phases are the primary reasons for formation damage measured as permeability impairment (Civan 2000, 2007; Galal et al. 2016). Moreover, formation damage is a catastrophic operational and financial issue during the many stages of oil and gas recovery from reservoirs, including drilling, production, hydraulic fracturing, and workover operations. According to Amaefule et al. (1993), formation is particularly prone to occur in poorly lithified and densely packed formations that contain significant amounts of authigenic, pore-filling clays that

are susceptible to aqueous solutions, such as kaolinite, illite, smectite, chlorite, and mixes-layer clay minerals. Accordingly, accurate identification of the dominant clay phase as well as prediction of their distribution patterns is crucial for optimal reservoir management. The PEF versus Th/K cross-plot reflects the clay composition in the studied sediments (Schlumberger 1985; Schon 2011). Most of the studied sediments have Th/K values less than 10 typifying that montmorillonite is the most dominant clay phase in the studied Cenomanian sediments (Fig. 14b). Potassium (K) and thorium (Th) contents confirm that clay minerals in the studied sediments are mainly represented by montmorillonite and mixed layer clays with subordinate contents of kaolinite and illite. The mixed clay phases mainly consist of mixed illite/smectite (Fig. 14c, d).

Thin bed analysis (TBA) was utilized to identify different forms of shale associated with sandstone reservoirs of the Bahariya Formation and Abu Roash G Member (Farrag et al. 2021). The Thomas–Stieber model was initially created to resolve the problem of laminated shaly sand sequences in the older South Louisiana fields. Shale exists in three different forms in the sand: dispersed, laminated, and structural (Ali et al. 2016; Schlumberger 2011; Willis et al. 2017). The gamma-ray and density porosity log values were plotted to determine the sand fraction, the sand porosity, and the shale distribution. Figure 15a typifies that the sandstone of the B-3 unit is marked by laminated shale and rare dispersed shale. Nevertheless, the B-2 and the B-1 units are marked by laminate shale only (Fig. 15b, c). On the other hand, A/R G is marked by laminated shale and rare structural shale (Fig. 15d).

Conclusions

The Cenomanian sediments host the most prolific reservoir targets in the north Western Desert. In the studied GPY oil field, the Cenomanian rock units were subdivided into four main units with variable lithologic and petrophysical characteristics. These units comprise Bahariya units (B-3, B-2, B-1) as well as the AR/G member. B-3 unit consists mainly of sandstone, siltstone, and little shale streaks with the presence of carbonate as cement and bed intercalation. The sand content decreases upward from B-3 to B-1 with an upward increase in the silt, shale, and carbonate content. AR/G consists preliminary of carbonate with little content of quartz and silicate minerals.

The depositional facies change upward from Clastics facies in B-3 to mixed siliciclastics carbonate B-1, B-2, and carbonate in AR/G. B-3 has the best reservoir characteristics and hosts the best reservoir conduits and the highest contents of hydrocarbon saturation. The reservoir conduits

are preferentially distributed in the southern part of the study region where the B-3 units have the highest values of porosity and lowest content of shale volume. The shale mineralogy consists mainly of smectite and mixed-layer illite/smectite and therefore induces a detrimental impact on the reservoir quality. Consequently, the facies of the lowest content of clays have the best reservoir quality. Therefore, the reservoir quality of the Cenomanian rock units decreases upward from B-3 to AR/G. Furthermore, the occurrence of shale streaks would be an effective seal for the hydrocarbon because of its dominant smectite content resulting in a very effective seal capacity.

Abbreviations Abbreviation: Complete name unit; SP: Spontaneous potential log mv; CALI/HCAL/CALX: Caliper log in; GR/HSGR: Gamma ray log, spectral gamma ray API; DT: Sonic log, compressional slowness, compensated sonic us/ft; RHOB/RHOZ/ZDNC: Formation density compensated logs, density log gm/cm3; APLC/CNCF/NPHI/CNL: Neutron log v/v; MSFL: Microsphirically focused log Ohm.m; LLD: Deep Laterolog; LLS: Shallow Laterolog; PEF: Photoelectric factor effect; VSH: Volume of shale %; PHIT_ND, $\varnothing$t: Neutron-density total porosity %; PHIE_ND, $\varnothing$e: Neutron-density effective porosity %; SWE_INDO: Water saturation-Indonesian %; Sh: Hydrocarbon saturation %; S_{hm}: Movable hydrocarbon saturation; TVDSS: True vertical depth subsea M; B-3: Bahariya-3; B-2: Bahariya-2; B-1: Bahariya-1; AR/G: Abu Roash G Member; GPY: General petroleum Y block; AG: Abu Gharadig basin; 2D: Two dimensional; K: Potassium; Th: Thorium; TBA: Thin bed analysis; F2: Fault number 2; C.I: Contour interval; MD: Measured depth M

Declarations The datasets generated during and/or analyzed during the current study are available from the corresponding author upon reasonable request.

Competing interests The authors declare no competing interests.

References

Abdel Maksoud A, Amin AT, El-Habaak GH, Ewida HF (2019) Facies and petrophysical modeling of the Upper Bahariya Member in Abu Gharadig oil and gas field, north Western Desert, Egypt. J African Earth Sci 149:503–516. https://doi.org/10.1016/j.jafrearsci.2018.09.011

Abdel-Fattah MI, Metwalli FI, Mesilhi ESI (2018) Static reservoir modeling of the Bahariya reservoirs for the oilfields development in South Um barka area, Western Desert, Egypt. J African Earth Sci 138:1–13. https://doi.org/10.1016/j.jafrearsci.2017.11.002

Abdel Maksoud YG, Abu-Zeid MM, El Aassy IE, Baghddady AR (2018) Lithostratigraphy, petrography and diagenesis of Um Bogma Formation in Talet Seleim area, southwestern Sinai. Egypt. Egyptian J Geol 62:233–246

Abu Shady AN, El-Shishtawy AM, Abdel Hameed AT, Abdel Kader TA (2010) Reservoir characterization of the upper cretaceous Bahariya Formation, Khalda ridge, North Western Desert, Egypt. 6th International Symposium on Geophysics, pp 34–46

Abu-Hashish MF, Said A (2016) Volumetric assessment through 3DGeostatic model for Abu Gharadig "G" Reservoir in Amana Field-East Abu Gharadig Basin-Western Desert-Egypt. J Geol Geophys 5(2):242. https://doi.org/10.4172/2381-8719.1000242

Ali A, Hussain MZ, Rehman K, Toqeer M (2016) Effect of shale distribution on hydrocarbon sands integrated with anisotropic rock physics for AVA modeling: a case study. Acta Geophys 64(4):1139–1163

Alsharhan AS, Abd El-Gawad EA (2008) Geochemical characterization of potential Jurassic/Cretaceous source rocks in the Shushan Basin, northern Western Desert, Egypt. J Pet Geol 31(2):191–212. https://doi.org/10.1111/j.1747-5457.2008.00416.x

Amaefule JO, Altunbay M, Tiab D, Kersey DG, Keelan DK (1993) Enhanced reservoir description: using core and log data to identify hydraulic (flow) units and predict permeability in uncored intervals/wells. SPE Annual Technical Conference and Exhibition, Houston, Texas, October 1993, pp 205–220. https://doi.org/10.2118/26436-MS

Bevan TG, Moustafa AR (2012) Inverted rift basin northern Egypt. Regional Geology and Tectonics: Phanerozoic Rift Systems and Sedimentary Basins. pp 482–507. https://doi.org/10.1016/B978-0-444-56356-9.00018-3

Bosworth W, El-Hawat AS, Helgeson DE, Burke K (2008) Cyrenaican "shock absorber" and associated inversion strain shadow in the collision zone of northeast Africa. Geology 36(9):695–698. https://doi.org/10.1130/G24909A.1

Bosworth W, Guiraud R, Kessler LG (1999) Late Cretaceous (ca 84 Ma) compressive deformation of the stable platform of northeast Africa (Egypt): far-field stress effects of the "Santonian event" and origin of the Syrian arc deformation belt. Geology 27(7):633–636. https://doi.org/10.1130/00917613(1999)027%3c0633:LCCMCD%3e2.3.CO;2

Bridge JS, Mackey SD (1993) A revised alluvial stratigraphy model. Alluvial sedimentation, pp 317–336. https://doi.org/10.1002/9781444303995.ch22

Bruke JA, Schmidt AW, Campbell RL (1969) The litho-porosity cross plot. A method for determining rock characteristics for computational log data. The log analyst SPWLA, 10(6), pp. 25–43 https://eurekamag.com/research/018/267/018267678.php

Chou YM, Song SR, Tsao TM, Lin CS, Wang MK, Lee JJ, Chen FJ (2014) Identification and tectonic implications of nano-particle quartz (< 50 nm) by synchrotron X-ray diffraction in the Chelungpu fault gouge, Taiwan. Tectonophysics 619:36–43. https://doi.org/10.1016/j.tecto.2013.07.021

Civan F (2000) Mechanism of clay swelling from reservoir formation damage: fundamentals, modeling, assessment, and mitigation. Elsevier. https://www.worldcat.org/title/reservoir-formation-damage-fundamentals-modeling-assessment-and-mitigation/oclc/471519315&referer=brief_results

Civan F (2007) Reservoir formation damage: fundamentals, modeling, assessment, and mitigation. Second Edition. USA: Burlington, pp 1–4. https://doi.org/10.1016/B978-0-7506-7738-7.X5000-3

Colombera L, Mountney NP, Hodgson DM, McCaffrey WD (2016) The Shallow-Marine Architecture Knowledge Store: a database for the characterization of shallow-marine and paralic depositional systems. Mar Pet Geol 75:83–99. https://doi.org/10.1016/j.marpetgeo.2016.03.027

Dolson JC, Shann MV, Matbouly SI, Hammouda H, Rashed RM (2001) Egypt in the twenty-first century: petroleum potential in offshore trends. GeoArabia 6(2):211–230. https://doi.org/10.2113/geoarabia0602211

EGPC (1992) Western Desert, oil and gas fields, a comprehensive overview. 11th EGPC Exploration and Production Conference, Cairo., pp 1–431. https://books.google.com.sa/books/about/Western_Desert_Oil_and_Gas_Fields.html?id=v6qDswEACAAJ&redir_esc=y

Ehrenberg SN (1990) Relationship between diagenesis and reservoir quality in sandstones of the Garn Formation, Haltenbanken, Mid-Norwegian Continental Shelf. AAPG Bullet (1990) 74(10):1538–1558. https://doi.org/10.1306/0C9B2515-1710-11D7-8645000102C1865D

El Adl H, Leila M, Ahmed MA, Anan T, El-Shahat A (2021) Integrated sedimentological and petrophysical rock-typing of the Messinian Abu Madi formation in South Batra gas field, onshore Nile Delta. Egypt Mar Petrol Geol 124:1–28

El Gazzar AM, Moustafa AR, Bentham P (2016) Structural evolution of the Abu Gharadig field area, northern Western Desert. Egypt. J Afr Earth Sci 124:340–354. https://doi.org/10.1016/j.jafrearsci.2016.09.027

El Mahdy M, Tarabees E, Bakr A, Farag AE (2019) Polygonal faults in Eocene carbonate reservoir, Abu El-Gharadig Basin, Egypt. Geol J 55(6):4670–4680. https://doi.org/10.1002/gj.3708

El-Shaarawy OA, Zaafan S, Rashed R, Lelek J, El Leboudy M, Hadidy A (1994) Jurassic hydrocarbon potentiality in the Abu Gharadig basin, North Western Desert of Egypt. 12th EGPC Explor. And Prod Conf Cairo 2:234–247

Farrag GH, Abd-Allah A, Bakr A, Hassan Z, El-Shahawy S (2022) Hydrocarbon potentiality of the Jurassic-Lower Cretaceous sequence in Abu Sennan area, Abu Gharadig Basin, Egypt. Arab J Geosci 15:1423. https://doi.org/10.1007/s12517-022-10660-y

Farrag GH, Baghdady A, Elnaggar OM (2021) Petrophysical attributes of the middle zone of the Bahariya Formation as a producing reservoir using core analysis correlations and log evaluation, Abu Sennan area, Egypt. J African Earth Sci 180:104225. https://doi.org/10.1016/j.jafrearsci.2021.104225

Galal SK, Elgibaly AA, Elsayed SK (2016) Formation damage due to fines migration and its remedial methods Egypt. J Petrol 25(4):515–524. https://doi.org/10.1016/j.ejpe.2015.11.005

Garfunkel Z (1998) Constrains on the origin and history of the Eastern Mediterranean basin. Tectonophysics 298(1–3):5–35. https://doi.org/10.1016/S0040-1951(98)00176-0

Garfunkel Z (2004) Origin of the Eastern Mediterranean basin: a reevaluation. Tectonophysics 391(1–4):11–34. https://doi.org/10.1016/j.tecto.2004.07.006

Ghassem AMK (2018) XRD evaluation of clay minerals in Shaley Formation and its comparison with cross plotting of log data. Progress Petrochem Sci 1(3):PPS.000513.3018. https://doi.org/10.31031/PPS.2018.01.000513

Ghassem AMK, Roozmeh A (2017) Determination of shale types using well logs. Int J Petrochem Sci Eng 2(5):160–166. https://doi.org/10.15406/ipcse.2017.02.00051

Guiraud R (1998) Mesozoic rifting and basin inversion along the northern African Tethyan margin: an overview. Geol Soc London Spec Publ 132(1):217–229. https://doi.org/10.1144/GSL.SP.1998.132.01.13

Guiraud R, Bosworth W (1997) Senonian basin inversion and rejuvenation of rifting in Africa and Arabia: synthesis and implications to plate-scale tectonics. Tectonophysics 282(1–4):39–82. https://doi.org/10.1016/S0040-1951(97)00212-6

Guiraud R, Bosworth W, Thierry J, Delplanque A (2005) Phanerozoic geological evolution of Northern and Central Africa: an overview. J African Earth Sci 43(1–3):83–143. https://doi.org/10.1016/j.jafrearsci.2005.07.017

Hantar G (1990) North Western Desert. In: The geology of Egypt. (Ed. R. Said, 1990). Balkema Publishers, pp 293–319

Helba AA, Bakry B (1996) Elusive traps revive prospectivity in mature basin Abu Roash 'F' case study, Abu Gharadig Basin, Western Desert, Egypt. EGPC 1:60–80

Henaish A, Ramadan F, Abd El Fatah MO, Saleh AH (2022) Interpretation and analysis of Upper Cretaceous structural features at GPY Field, Western Desert, Egypt. Bulletin of Faculty of Science, Zagazig University (BFSZU), Vol 2022, Issue 4, p 13

Ibrahim MIA, Dilcher D, Kholeif S (2009) Palynomorph succession and paleoenvironment in the upper cretaceous Abu Gharadig oil field, northwestern desert, Egypt. Micropaleontology 55(6):525–558. https://www.jstor.org/stable/40607068

Jiang S (2012) Clay minerals from the perspective of oil and gas exploration. Clay minerals in nature-their characterization, modification and application, pp 21–38

Kassab MA, Abbas AE, Attiya AS (2019) Hydrocarbon potential of Upper Bahariya member in Um Baraka oil field, North Western Desert, Egypt. NRIAG J Astron Geophys 8(1):204–219. https://doi.org/10.1080/20909977.2019.1664542

Kitchka AA, Arkhipova SL, Bezkhyzhko OM, Kuzmenko PM, Makeev VV, Shevchenko OA, Bashkirov GL, Vakarchuk SG (2015) Tectonic sedimentary evolution of the Abu Gharadig basin and exploration challenges for the Western Desert province, Egypt. 14th International Conference on Geoinformatics: Theoretical and Applied Aspects, 11–14 May, Kiev, Ukraine. https://doi.org/10.3997/2214-4609.201412432

Leila M, Mohamed A (2020) Diagenesis and petrophysical characteristics of the shallow Pliocene sandstone reservoirs in the Shinfas Gas Field, onshore Nile Delta, Egypt. J Petrol Explor Prod Technol 10:1–19

Leila M, Moscariello A, Segvic B (2018) Geochemical constraints on the provenance and depositional environment of the Messinian sediments, onshore Nile Delta, Egypt: implications for the late Miocene paleogeography of the Mediterranean. J African Earth Sci 143:215–241

Leila M (2019) Clay minerals distribution in the pre-, syn-Messinian salinity crisis sediments of the onshore Nile Delta, Egypt: mineral origin and implications on the reservoir quality. J Afr Earth Sci 154:35–48

Leila M, El-Sheikh I, Abdel maksoud A, Radwan AA (2022a) Seismic sequence stratigraphy and depositional evolution of the Cretaceous-Paleogene sedimentary successions in the offshore Taranaki Basin, New Zealand: implications for hydrocarbon exploration. Mar Geophys Res 43:23. https://doi.org/10.1007/s11001-022-09483-z

Leila M, Yasser A, El Bastawesy M, El Mahmoudi A (2022b) Seismic stratigraphy, sedimentary facies analysis and reservoir characteristics of the Middle Jurassic syn-rift sediments in Salam Oil Field, north Western Desert, Egypt. Mar Pet Geol V 136. https://doi.org/10.1016/j.marpetgeo.2021.105466

Li S, Henderson CM, Stewart RR (2004) Well log study and stratigraphic correlation of the Cantuar Formation, southwestern Saskatchewan, CREWES Res. Rep. 16, pp 1–18. https://www.crewes.org/Documents/ResearchReports/2004/2004–01.pdf

Longacre M, Bentham P, Hanbal I, Cotton J, Edwards R (2007) New crustal structure of the Eastern Mediterranean basin: detailed integration and modeling of gravity, magnetic, seismic refraction, and seismic reflection data. In EGM 2007 International Workshop (pp cp-166).European Association of Geoscientists & Engineers. https://doi.org/10.3997/2214-4609-pdb.166.D_OP_07

Loucks RG, Marianne MD, William EG (1984) Regional controls on diagenesis and reservoir quality in lower Tertiary sandstones along the Texas Gulf Coast. In: Part 1. Concepts and principles. American Association of Petroleum Geologists, pp 15–45. https://doi.org/10.1306/M37435C2

Mitchum Jr, R M, Vail PR, Sangree JB (1977) Seismic stratigraphy and global changes of sea level: part 6. Stratigraphic interpretation of seismic reflection patterns in depositional sequences: Section 2. Application of seismic reflection configuration to stratigraphic interpretation, pp 117–133

Mohamed AK, Ghazala HH, Mohamed L (2016) Integration between well logging and seismic reflection techniques for structural analysis and reservoir characterizations, Abu El Gharadig basin, Egypt. NRIAG J Astron Geophys 5(2):362–379. https://doi.org/10.1016/j.nrjag.2016.07.003

Mousa AS, El-Hariri TY, Abu El-Ezz AR (2011) A study of microfacies and petrophysical analysis of some subsurface Cretaceous rocks of Abu Gharadig-34 Well, Western Desert, Egypt. Petrol Sci Technol 29(22):2306–2320. https://doi.org/10.1080/10916461003663081

Moustafa AR (2008) Mesozoic-Cenozoic basin evolution in the northern Western Desert of Egypt, In: Solem, M., EI-Arnouti, A., and Saleh, A. (eds), 3fd Symposium on the sedimentary basins of Libya (The Geology of East Libya), v 3, pp 29–46

Moustafa AR, Khalil MH (1990) Structural characteristics and tectonic evolution of the North Sinai fold belt. In: The Geology of Egypt. AA Balkema, Rotterdam, pp 381–389

Nabawy BS, El Sharawy MS (2015) Hydrocarbon potential, structural setting and depositional environments of Hammam Faraun Member of the Belayim Formation, Southern Gulf of Suez, Egypt. J African Earth Sci 112:93–110

Pittman ED (1992) Relationship of porosity and permeability to various parameters derived from mercury injection-capillary pressure curves for sandstone. AAPG Bullet Am Assoc Petrol Geol 76(2):191–198

Posamentier HW, Allen GP (1999) SiliciClastics sequence stratigraphy. Concepts Appl: SEPM Concepts Sedimentol Paleontol 7:210

Radwan AA, Abdelwahhab MA, Nabawy BS, Mahfouz KH, Ahmed MS (2022) Facies analysis-constrained geophysical 3D-static reservoir modeling of Cenomanian units in the Aghar Oil field (Western Desert, Egypt): insights into paleoenvironment and petroleum geology of fluviomarine systems. Mar Pet Geol 136:105436. https://doi.org/10.1016/j.marpetgeo.2021.105436

Saleh AH, Farag AE, and Eysa EA (2021) Reservoir quality of Abu Roash (G) member in Karama Oil Field, East Bahariya Concession, North Western Desert, Egypt. Arabian J Geosci 14(3):169. https://link.springer.com/article/10.1007/s12517-020-06349-9

Sarhan MA (2017) Seismic-wireline logs sequence stratigraphic analyses and geologic evolution for the Upper Cretaceous succession of Abu Gharadig basin, Egypt. J Afr Earth Sci 129:469–480. https://doi.org/10.1016/j.jafrearsci.2017.02.004

Schlumberger (1974) Log interpretation principles/application. Houston, tex, Schlumberger.2, 87. https://www.worldcat.org/title/loginterpretationprinciplesapplications/oclc/890820436&referer=brief_results

Schlumberger (2011) Tech log manual of thin-bed(TBA). Schlumberger well services Inc, Houston

Schlumberger (1985) Well evaluation conference. Schlumberger Well Services Inc, Nigeria, p 290

Schlumberger (1995) Well evaluation conference, Egypt. Schlumberger Technical Editing Services, Chester, pp 58–66

Schon SC (2011) Hydraulic fracturing not responsible for methane migration. Proc Natl Acad Sci 108(37):E664–E664. https://doi.org/10.1073/pnas.1107960108

Shazly TF, Nouh AZ (2013) Determination of some reservoir characteristics of the Bahariya Formation in Bed-1 Field, Western Desert, Egypt, by using the repeat formation tester. Pet Sci Technol 31(7):763–774. https://doi.org/10.1080/10916466.2010.531603

Spooner P (2018) Lifting the fog of confusion surrounding total and effective porosity Petrophysics. SPWLA 59thAnnual Logging symposium , London, UK, 2018. https://onepetro.org/SPWLAALS/proceedings-abstract/SPWLA18/4-SPWLA18/D043S006R005/28832

Stampfli GM, Borel GD, Cavazza W, Mosar J, Ziegler PA (2001) Palaeotectonic and palaeogeographic evolution of the western Tethys and PeriTethyan domain (IGCP Project 369). Episodes J Int Geosci 24(4):222–228. https://doi.org/10.18814/epiiugs/2001/v24i4/001

Tassy A, Crouzy E, Gorini C, Rubino JL, Bouroullec JL, Sapin F (2015) Egyptian Tethyan margin in the Mesozoic: evolution of a mixed carbonate-siliciClastics shelf edge (from Western Desert to Sinai). Mar Pet Geol 68:565–581. https://doi.org/10.1016/j.marpetgeo.2015.10.011

Tearpock, DJ, Bischke RE (1991) Applied subsurface geological mapping, Englewood Cliffs, NJ, Prentice-Hall, https://www.worldcat.org/title/applied-subsurface-geologicalmapping/oclc/246563669&referer=brief_results

Teama MA, Nabawy BS (2016) Petrophysical evaluation of the hydrocarbon potential of the Lower Cretaceous Kharita clastics North Qarun oil field, Western Desert, Egypt. J African Earth Sci 121:62–71

Temraz MGM, Abdou AA, Shehata MG (2009) Sedimentology of the Bahariya Formation in Salam-IX Well, Northern Western Desert, Egypt. Pet Sci Technol 27(14):1621–1636. https://doi.org/10.1080/10916460802608222

Thomas EC, Stieber US (1975) The distribution of shale in sandstones and its effect upon porosity. Paper presented at the SPWLA 16th annual logging symposium. New Orleans, Louisiana, June1975 https://onepetro.org/SPWLAALS/proceedings-abstract/SPWLA-1975/All-SPWLA-1975/SPWLA-1975-T/20024

Tian Y, He E, Chen H, Wang H, Yuan H, Zhang Y, Liu S (2018) Petrology, lithofacies, and sedimentary environment of Upper Cretaceous Abu Roash "G" in the AESW Block, Abu Gharadig Basin, Western Desert, Egypt. J African Earth Sci 145:178–189. https://doi.org/10.1016/j.jafrearsci.2018.05.017

Walderhaug O, Eliassen A, Aase NE (2012) Prediction of permeability in quartz-rich sandstones: examples from the Norwegian Continental Shelf and the Fontainebleau Sandstone. J Sediment Res 82(12):899–912. https://doi.org/10.2110/jsr.2012.79

Wei Y, Jianbo W, Shuai L, Kun W, Yinan Z (2014) Logging identification of the Longmaxi mud shale reservoir in the Jiaoshiba area. Sichuan Basin Nat Gas Ind B 1(2):230–236. https://doi.org/10.1016/j.ngib.2014.11.016

Wescott WA, Atta M, Blanchard DC, Georgeson ST, Miller DA, Walter WO, Welson AD, Dolson JC, Sehim A (2011) Jurassic rift Architecture in the Northeastern Western Desert, Egypt. AAPG international conferecnce and exhibition, Milan, Italy, pp 23–26

Willis JJ, McIntosh DS, Zwenne SJW, Ferguson GJ (2017) Quick-look technique for quantifying shale distribution types using total porosity versus shale volume cross plots: Gulf Coast Association of Geological Societies Transactions, v 67, pp 539 -549. https://archives.datapages.com/data/gcags/data/067/067001/539_gcags670539.htm

Yasser A, Leila M, El Bastawesy M, El Mahmoudi A (2021) Reservoir heterogeneity analysis and flow unit characteristics of the Upper Cretaceous Bahariya Formation in Salam Field, north Western Desert, Egypt. Arab J Geosci 14:1635. https://doi.org/10.1007/s12517-021-07985-5